Available online at www.sciencedirect.com
ScienceDirect
Journal of Computational Physics 221 (2007) 88–105
JOURNAL OF COMPUTATIONAL PHYSICS
www.elsevier.com/locate/jcp

The 3D wave equation and its Cartesian coordinate stretched perfectly matched embedding – A time-domain Green's function performance analysis

Adrianus T. de Hoop *, Robert F. Remis, Peter M. van den Berg [1]

Laboratory of Electromagnetic Research, Faculty of Electrical Engineering, Mathematics and Computer Science, Delft University of Technology, Mekelweg 4, 2628 CD Delft, The Netherlands

Received 3 May 2005; received in revised form 2 June 2006; accepted 4 June 2006
Available online 28 July 2006

Abstract

A general class of 3D perfectly matched, i.e., reflectionless, Cartesian embeddings (perfectly matched layers in the three coordinate directions) is analyzed with the aid of a combined time-domain Green's function technique and a time-domain, causality-preserving, Cartesian coordinate stretching procedure. It is shown that, for an unbounded embedding of the specified class, the wavefield is, in any 3-rectangular computational solution domain, reproduced exactly. The spurious reflection caused by a (computationally necessary) truncation of the embedding is analyzed as a function of layer thicknesses and their coordinate stretching relaxation functions. A time-domain uniqueness proof for the solution to the truncated embedding problem is provided and a numerical illustration is given for a test case with known analytical solution. For such cases, the pure space-time discretization errors can be separated from the disturbance caused by the spurious reflection. For the second-order coordinate stretched wave equation an equivalent system of first-order equations is presented.

MSC: 65C20; 65M12; 65N12; 65G99

PACS: 02.60.−x; 03.40.Kf; 07.05.T

Keywords: Computational modeling; Perfectly matched embeddings; Time-domain wavefield computation

1. Introduction

The computation of transient wavefields in unbounded space takes typically place by discretizing the relevant space-time partial differential equations in some *solution domain* of bounded support, in conjunction with

* Corresponding author. Tel.: +31 15 2785203; fax: +31 15 2786194.
E-mail addresses: a.t.dehoop@ewi.tudelft.nl (A.T. de Hoop), r.f.remis@ewi.tudelft.nl (R.F. Remis), p.m.vandenberg@tnw.tudelft.nl (P.M. van den Berg).
[1] Presently at Department of Imaging Science and Technology, Faculty of Applied Sciences, Delft University of Technology, Lorentzweg 1, 2628 CJ Delft, The Netherlands.

0021-9991/$ - see front matter
doi:10.1016/j.jcp.2006.06.018

a computational procedure that somehow mimicks a reflectionless radiation into the solution domain's *embedding*. Three different methods to account for the latter can be distinguished. In the first, the dimensions of the solution domain are chosen so large that the generated wave motion has, in the time window of computation, not yet reached the boundary surface. In this case the wave function values can, at the boundary of the solution domain, be put equal to zero. This method can, in most practical cases, only be used in time windows of sufficiently small duration. In the second method, so-called *absorbing boundary conditions* are invoked on the boundary of the solution domain. Such absorbing boundary conditions fall into two categories: exact ones and approximate ones. The exact ones are based on some integral or series representation of the wavefield in the embedding, the integrands or coefficients in which are interrelated to the wavefield's boundary values. Conditions of this type are of a non-local nature and destroy the sparseness of the system's matrix associated with the discretization of the differential operator involved. Absorbing boundary conditions of a local nature (in which the sparseness of the system's matrix is preserved) do exist, but they are of an approximate nature and, as a rule, they do not perform well off the normal to, and in the neighborhood of, the boundaries on which they are invoked [22,23]. A third method aims to construct differential equations that coincide with the equations that describe the wave motion under consideration in the solution domain, but that enforce an excess time delay and/or an excess decay of their solution away from the boundary into the embedding, without disturbing the solution in the solution domain. Such artificial embeddings are denoted as *perfectly matched* or *reflectionless*. The present paper shows how to construct analytically, for a solution domain in the shape of a 3-rectangle, a rather general class of such space-time 3D, Cartesian, perfectly matched embeddings. The basic ingredient in it is a convolutional, causality preserving, time-domain Cartesian coordinate stretching procedure, a special case of which (similar to the sub-class considered in Sections 7 and 9 of the present paper) has also been discussed by Chew and Weedon [16, Eqs. (46)–(51)] (see also [14]) and Rappaport [43,42]. Chew and Weedon start from the frequency-domain counterpart in an electromagnetic setting and arrive at 'Berenger'-type time-domain equations. In this respect it is observed that, although the frequency-domain version can serve as a guideline to the time-domain one, the condition of causality is an extra condition, necessitated for the uniqueness of the time-domain coordinate-stretched problem. Other approaches have been presented in [18,27,28] in connection with the scalar wave equation, [10,40,53] in connection with wave propagation problems in acoustics, [3,7,11–13,16,29,35,39,41] in connection with electromagnetics, and [10,15,26,30,31,34,38] in connection with elastodynamics.

Now, any computational implementation of perfectly matched embeddings requires their truncation by an outer boundary on which either Dirichlet or Neumann conditions are imposed on the wavefield. Such a truncation leads to the generation of *spuriously reflected waves* in the solution domain. To investigate the latter's properties on the wave phenomenon in the solution domain, we construct the time-domain Green's function for a configuration with arbitrary relaxation-type stretching functions along the three Cartesian coordinate directions, truncated with a Dirichlet boundary (Fig. 1). To gain insight into the relative influence of all the parameters and profiles involved, we provide a test case whose Green's function solution is constructed entirely analytically, thus concentrating on the mathematical properties of the embedding procedure. Furthermore, a 1D numerical experiment is reported where the pure space-time discretization errors in the presence of an absorptive layer with prescribed attenuation are isolated from the ones associated with the spurious reflection properties of the truncated perfectly matched embedding.

The heuristic idea behind the procedure originates from Berenger [7], who, in a perfectly matched layer (PML) added some non-physical components to the original field ones and extended the system of partial differential equations accordingly (see also the survey paper [50]). A stability analysis of the initial-value problem related to the thus extended system of equations, carried out in [1], shows that this problem is not strongly well-posed. Concurrently to this approach, a complex frequency-domain *coordinate stretching procedure* was introduced [11,13,16] (see also the review by Kozuoglu and Mittra [35], as well as the surveys in [24,47,48]). Here, frequency-domain, non-reflecting plane-wave arguments stand at the basis of the construction of one-dimensional perfectly matched layers (PML's) out of which three-dimensional, Cartesian, perfectly matched embeddings are built that bound the solution domain. This procedure leaves open the questions about the three-dimensional properties of the configuration solution domain plus embedding (in particular near and at the intersections of the planar layers: i.e., edges and corners) as well as the uniqueness and causality properties of the solution to the differential equation that replaces the wave equation in the embedding.

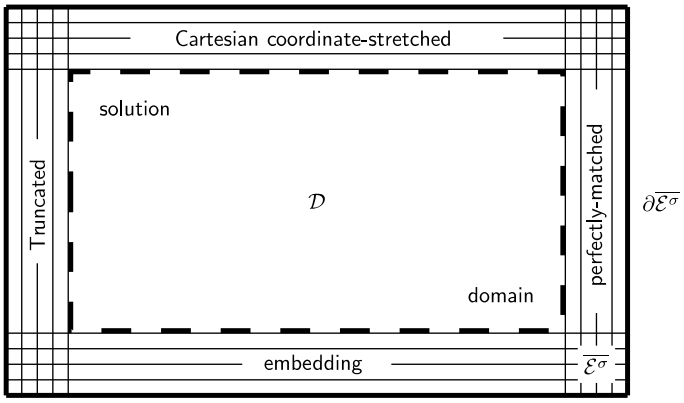

Fig. 1. Bounded solution domain $\mathscr{D}$ surrounded by truncated Cartesian coordinate-stretched perfectly-matched embedding $\overline{\mathscr{E}^\sigma}$.

Typically, the further standard procedure is to construct the relevant differential equation(s) and subsequently investigate the properties of their solution through numerical experiments. Our derivation proceeds differently and is based on the three-dimensional pertaining space-time integral representation for the wavefield in the entire configuration consisting of solution domain and unbounded embedding, and specifically on the properties of the space-time Green's function in this configuration. The class of space-time coordinate stretching functions that we construct is shown to yield unique and causal solutions, not only for the corresponding unbounded embeddings with outgoing waves, but also for the computationally required truncated ones, supplied with Dirichlet or Neumann type of boundary conditions. The class of wave functions under consideration is a solution of a rather general dissipative wave equation, the coefficients in which contain relaxation functions of the Boltzmann type [17]. To guarantee uniqueness of the relevant initial-value problem, these relaxation functions have to meet certain causality and stability conditions [17, Section 2.2]. Since our time-domain stretching functions are taken to satisfy conditions of a similar type, it is conjectured that our class of time-domain stretching functions does also lead to stable systems of discretized equations, but the aspect of stability itself in all generality remains to be investigated. (For procedures in this direction, see [6,25,49].)

Although the time convolutions in the coordinate-stretched differential equations can be handled numerically (for example, by the Newmark method [32,33]), the alternative procedure of constructing a system of supplementing differential equations such that a consistent first-order coupled system arises, is often preferred. For the subclass of space-time coordinate stretching functions that lead to time delay and/or absorption in the embedding, we present such a system via the straightforward application of some rules of the unilateral time Laplace transformation. To demonstrate the practical use of the system, a 1D numerical experiment is carried out, in which, owing to the availability of an exact solution, the pure space-time discretization errors can be separated from the disturbance associated with the spuriously reflected wave.

The 3D coordinate-stretched embedding is, apart from the spurious reflections due to its truncation, exactly perfectly matched for 3-rectangles only. As is shown, this is a consequence of the property that in rectangular coordinates the Green's function only depends on the differences of the coordinates of source point and observation point. In other coordinate systems, for example, cylindrical and spherical ones, a coordinate stretching procedure can, since the Green's function in those systems has no such simple structure, not lead to a perfectly matched embedding, and one must rely on approximate procedures. Since through the Green's function procedure a guaranteed attenuation of the, truncation generated, spuriously reflected waves can be established, one can, in all practical applications, restrict the actual 'solution domain' (Fig. 1) to the minimum required by the problem at hand.

2. Description of the wave motion in the configuration

We consider transient scalar wavefields that are to be computationally modeled in a bounded subdomain $\mathscr{D}$ (the *solution domain*) of three-dimensional Euclidean space $\mathbb{R}^3$. The closed boundary surface of $\mathscr{D}$ is $\partial\mathscr{D}$. The

complement of $\mathscr{D} \cup \partial\mathscr{D}$ in $\mathbb{R}^3$ is denoted as the *embedding* $\mathscr{D}^\infty$. Position in the configuration is specified by the coordinates $\{x, y, z\}$ with respect to an orthogonal, Cartesian reference frame with the origin $\mathscr{O}$ and the three mutually perpendicular base vectors $\{\boldsymbol{i}_x, \boldsymbol{i}_y, \boldsymbol{i}_z\}$, each of which is of unit length. In the indicated order, the base vectors form a right-handed system. Whenever appropriate, the position is also specified by the position vector $\boldsymbol{r} = x\boldsymbol{i}_x + y\boldsymbol{i}_y + z\boldsymbol{i}_z$. The time coordinate is t. Partial differentiation is denoted by ∂, supplied with the relevant subscript.

The wave motion is characterized by the scalar wave function $u(\boldsymbol{r}, t) = u(x, y, z, t)$. In conformity with our procedure of constructing a perfectly matched embedding, this wave function is, in the solution domain, taken to satisfy a scalar wave equation of the type (dissipative wave equation)

$$\mathsf{D}u \stackrel{\text{def}}{=} \partial_x[\mu_x \overset{(t)}{*} \partial_x u] + \partial_y[\mu_y \overset{(t)}{*} \partial_y u] + \partial_z[\mu_z \overset{(t)}{*} \partial_z u] - c^{-2}\kappa \overset{(t)}{*} \partial_t^2 u = -Q^{\text{i}} \quad \text{for } \boldsymbol{r} \in \mathscr{D}, t \in \mathbb{R}, \tag{1}$$

where $\overset{(t)}{*}$ denotes time convolution, $\mu_{x,y,z}(\boldsymbol{r}, t)$ and $\kappa(\boldsymbol{r}, t)$ are normalized, passive, causal relaxation functions of the Boltzmann type, c is the wavespeed of the embedding (a positive constant) and $Q^{\text{i}}(\boldsymbol{r}, t)$ is the volume source density of the exciting sources. It is assumed that $\text{supp}(Q^{\text{i}}) \subset \mathscr{D}$, in which domain Q^{i} is a piecewise continuous function of $\boldsymbol{r}$ and t. As to the coefficients $\mu_{x,y,z}(\boldsymbol{r}, t)$ and $\kappa(\boldsymbol{r}, t)$ occurring in the differential operator D, we assume that they are piecewise continuous functions of $\boldsymbol{r}$ and, apart from a Dirac delta distribution term operative at $t = 0$ (yielding the instantaneous response), continuous functions of t that vanish for $t < 0$ (causality requirement). They are representative for the constitutive properties of the medium in which the wave propagates and may show finite jumps across a finite number of surfaces on which the unit vector $\boldsymbol{\nu}$ along the normal is piecewise continuous. Across these surfaces of jump discontinuity in medium properties, the wave function u and the linear combination $\nu_x[\mu_x \overset{(t)}{*} \partial_x u] + \nu_y[\mu_y \overset{(t)}{*} \partial_y u] + \nu_z[\mu_z \overset{(t)}{*} \partial_z u]$ of its first-order derivatives are to be continuous. Eq. (1) arises, for example, as the scalar wave equation satisfied by the acoustic pressure of an acoustic wavefield in a lossy fluid with anisotropic inertia properties [19, pp. 34–35].

In the embedding of the solution domain, the wave function is taken to satisfy the sourcefree three-dimensional scalar wave equation

$$\mathsf{D}^\infty u \stackrel{\text{def}}{=} \partial_x^2 u + \partial_y^2 u + \partial_z^2 u - c^{-2}\partial_t^2 u = 0 \quad \text{for } \boldsymbol{r} \in \mathscr{D}^\infty, t \in \mathbb{R}. \tag{2}$$

i.e., in the embedding all relaxation functions reduce to $\delta(t)$.

The problem posed by the differential equations (1) and (2), the interface continuity conditions, the initial conditions $u(\boldsymbol{r}, 0) = 0$ and $\partial_t u(\boldsymbol{r}, 0) = 0$ for $\boldsymbol{r} \in \mathbb{R}^3$, together with the condition that, in the embedding, the wave motion consists of outgoing waves only, has a solution that exists and is unique (see [20,21]).

To express the behavior of the wave function in terms of the Green's function associated with Eq. (2), we introduce the volume density $Q^{\text{s}}(\boldsymbol{r}, t)$ of *contrast sources* with respect to the embedding via

$$-Q^{\text{s}} \stackrel{\text{def}}{=} \mathsf{D}^\infty u - \mathsf{D}u \quad \text{for } \boldsymbol{r} \in \mathbb{R}^3, \ t \in \mathbb{R}. \tag{3}$$

Note that Q^{s} is uniquely determined and that its support is obviously the bounded subdomain of $\mathscr{D}$ where the relaxation functions in D differ from their values in the embedding. Upon combining Eqs. (1) and (3) we obtain the equation

$$\mathsf{D}^\infty u = -Q^{\text{i}} - Q^{\text{s}} \quad \text{for } \boldsymbol{r} \in \mathbb{R}^3, \ t \in \mathbb{R}. \tag{4}$$

This equation implies that u is related to the right-hand side via

$$u(\boldsymbol{r}, t) = \int_{\mathscr{D}} G(\boldsymbol{r}, \boldsymbol{r}', t) \overset{(t)}{*} [Q^{\text{i}}(\boldsymbol{r}', t) + Q^{\text{s}}(\boldsymbol{r}', t)] \, \mathrm{d}V(\boldsymbol{r}') \quad \text{for all } \boldsymbol{r} \in \mathscr{R}^3, \ t \in \mathbb{R}, \tag{5}$$

in which

$$G(\boldsymbol{r}, \boldsymbol{r}', t) = \frac{\delta(t - R/c)}{4\pi R} \quad \text{for } R \neq 0, \tag{6}$$

with

$$R = [(x - x')^2 + (y - y')^2 + (z - z')^2]^{1/2} \geqslant 0, \tag{7}$$

is the causal free-space Green's function associated with the differential operator D^{∞}. Eqs. (5)–(7) will serve as the basis for our construction of a general class of absorptive and dispersive, perfectly matched, i.e. reflectionless, computational counterparts of the embedding $\mathscr{D}^{\infty}$.

The relevant construction takes place via the time Laplace transformation of the causal time functions involved. Let $t = 0$ be the instant at which the activating sources start to act, then the generated wavefield vanishes everywhere in space for $t < 0$ and its (unilateral) time Laplace transform is given by

$$\hat{u}(\boldsymbol{r}, s) = \int_{t=0}^{\infty} \exp(-st) u(\boldsymbol{r}, t)\, \mathrm{d}t \quad \text{for } \boldsymbol{r} \in \mathbb{R}^3. \tag{8}$$

Restricting ourselves to the physically and computationally important case of bounded wavefield values, the right-hand side of Eq. (8) exists in the right half $\{s \in \mathbb{C}, \mathrm{Re}(s) > 0\}$ of the complex s-plane, where it is an analytic function of the complex variable s. For the rest of the analysis we take s to be on the positive real s-axis and rely for the unique correspondence between $\hat{u}(\boldsymbol{r}, s)$ and $u(\boldsymbol{r}, t)$ on Lerch's uniqueness theorem. This theorem states that to the sequence $\{\hat{u}(\boldsymbol{r}, s_n); s_n = s_0 + nh, s_0 > 0, h > 0, n = 0, 1, 2, \ldots\}$ there corresponds only one $u(\boldsymbol{r}, t)$ that vanishes for $t < 0$ [52]. Since under the transformation, together with zero-value initial conditions, $\hat{\partial}_t = s, \hat{u}$ satisfies the equation

$$\widehat{\mathsf{D}}^{\infty}\hat{u} \stackrel{\text{def}}{=} \partial_x^2\hat{u} + \partial_y^2\hat{u} + \partial_z^2\hat{u} - (s^2/c^2)\hat{u} = -\widehat{Q}^{\mathrm{i}} - \widehat{Q}^{\mathrm{s}} \quad \text{for } \boldsymbol{r} \in \mathbb{R}^3, \tag{9}$$

while the representation (5) transforms into

$$\hat{u}(\boldsymbol{r}, s) = \int_{\mathscr{D}} \widehat{G}(\boldsymbol{r}, \boldsymbol{r}', s)[\widehat{Q}^{\mathrm{i}}(\boldsymbol{r}', s) + \widehat{Q}^{\mathrm{s}}(\boldsymbol{r}', s)]\, \mathrm{d}V(\boldsymbol{r}') \quad \text{for all } \boldsymbol{r} \in \mathbb{R}^3, \tag{10}$$

with

$$\widehat{G}(\boldsymbol{r}, \boldsymbol{r}', s) = \frac{\exp(-sR/c)}{4\pi R} \quad \text{for } R \neq 0. \tag{11}$$

These equations form the starting point of our further analysis.

3. The space-time Cartesian coordinate stretching procedure

Guided by the notion that relaxation (i.e., absorption and dispersion) in a linear, passive, time-invariant medium can mathematically be modeled via causal relaxation functions whose time Laplace transform is analytic in the right half of the complex s-plane, while being real-valued and positive on the positive real s-axis, we introduce three such functions, $\hat{\chi}_x(x, s), \hat{\chi}_y(y, s)$ and $\hat{\chi}_z(z, s)$, each of which satisfies these conditions. Furthermore, $\hat{\chi}_x(x, s)$ is assumed to be piecewise continuous in x, $\hat{\chi}_y(y, s)$ piecewise continuous in y, and $\hat{\chi}_z(z, s)$ piecewise continuous in z. The time-domain counterparts of these functions are to play the role of time-domain *Cartesian coordinate stretching functions*. Next, we investigate the properties of the function

$$\hat{u}^{\sigma}(\boldsymbol{r}, s) = \int_{\mathscr{D}} \widehat{G}^{\sigma}(\boldsymbol{r}, \boldsymbol{r}', s)[\widehat{Q}^{\mathrm{i}}(\boldsymbol{r}', s) + \widehat{Q}^{\mathrm{s}}(\boldsymbol{r}', s)]\, \mathrm{d}V(\boldsymbol{r}') \quad \text{for all } \boldsymbol{r} \in \mathbb{R}^3, \tag{12}$$

where

$$\widehat{G}^{\sigma}(\boldsymbol{r}, \boldsymbol{r}', s) = \frac{\exp(-s\hat{R}^{\sigma}/c)}{4\pi\widehat{R}^{\sigma}} \quad \text{for } \widehat{R}^{\sigma} \neq 0, \tag{13}$$

in which

$$\widehat{R}^{\sigma} = (\widehat{X}^2 + \widehat{Y}^2 + \widehat{Z}^2)^{1/2} \geqslant 0, \tag{14}$$

with the three *s-domain stretched Cartesian coordinates*

$$\widehat{X} = \int_{x'}^{x} \hat{\chi}_x(\xi, s)\, \mathrm{d}\xi, \quad \widehat{Y} = \int_{y'}^{y} \hat{\chi}_y(\eta, s)\, \mathrm{d}\eta, \quad \widehat{Z} = \int_{z'}^{z} \hat{\chi}_z(\zeta, s)\, \mathrm{d}\zeta. \tag{15}$$

Obviously, in each 3-rectangle of space that contains both $\boldsymbol{r}' = \{x', y', z'\}$ and $\boldsymbol{r} = \{x, y, z\}$ and in the interior of which $\hat{\chi}_x(x,s) = 1, \hat{\chi}_y(y,s) = 1$ and $\hat{\chi}_z(z,s) = 1$, we have $\widehat{R}^\sigma = R$. Since, further, $\widehat{Q}^{\mathrm{i}}$ and $\widehat{Q}^{\mathrm{s}}$, are fully determined by the original problem stated in Section 2, we then have in such a 3-rectangle $\hat{u}^\sigma = \hat{u}$, i.e., $\hat{u}$ is reproduced exactly, irrespective of how the values of $\hat{\chi}_x(x,s)$, $\hat{\chi}_y(y,s)$ and $\hat{\chi}_z(z,s)$ are, within the specified class, chosen outside that 3-rectangle. This opens the possibility to select the values of the coordinate stretching functions such that, outside the relevant 3-rectangle, $\hat{u}^\sigma$ as given by Eq. (12) is either strongly attenuated or strongly time-delayed, or both. These properties can then be exploited to truncate the domain in which the differential equation satisfied by the expression (12) is solved computationally. For this to be of practical use, we need the differential equation satisfied by $\hat{u}^\sigma$ or, which is equivalent, the differential equation satisfied by $\widehat{G}^\sigma$.

From the standard theory of the scalar wave equation it is known that $\widehat{G}^\sigma$ is the bounded solution as $\widehat{R}^\sigma \to \infty$ of the differential equation

$$\partial^2_{\widehat{X}} \widehat{G}^\sigma + \partial^2_{\widehat{Y}} \widehat{G}^\sigma + \partial^2_{\widehat{Z}} \widehat{G}^\sigma - (s^2/c^2)\widehat{G}^\sigma = -\delta(\widehat{X}, \widehat{Y}, \widehat{Z}). \tag{16}$$

Note that, due to the fact that s, and also the coordinate stretching functions, are real and positive, no difficulty in the interpretation of either the spatial derivatives or the Dirac delta distribution arises. Observing that

$$\partial_{\widehat{X}} = \hat{\chi}_x(x,s)^{-1}\partial_x, \quad \partial_{\widehat{Y}} = \hat{\chi}_y(y,s)^{-1}\partial_y, \quad \partial_{\widehat{Z}} = \hat{\chi}_z(z,s)^{-1}\partial_z \tag{17}$$

and

$$\delta(\widehat{X}, \widehat{Y}, \widehat{Z}) = [\hat{\chi}_x(x,s)\hat{\chi}_y(y,s)\hat{\chi}_z(z,s)]^{-1}\delta(x-x', y-y', z-z'), \tag{18}$$

Eq. (16) leads to

$$\begin{aligned}&\hat{\chi}_x^{-1}\partial_x(\hat{\chi}_x^{-1}\partial_x\widehat{G}^\sigma) + \hat{\chi}_y^{-1}\partial_y(\hat{\chi}_y^{-1}\partial_y\widehat{G}^\sigma) + \hat{\chi}_z^{-1}\partial_z(\hat{\chi}_z^{-1}\partial_z\widehat{G}^\sigma) - (s^2/c^2)\widehat{G}^\sigma\\ &\quad = -[\hat{\chi}_x\hat{\chi}_y\hat{\chi}_z]^{-1}\delta(x-x', y-y', z-z').\end{aligned} \tag{19}$$

In those domains where $\hat{\chi}_x = 1, \hat{\chi}_y = 1,\ \hat{\chi}_z = 1$, this equation reduces to

$$\partial_x^2\widehat{G} + \partial_y^2\widehat{G} + \partial_z^2\widehat{G} - (s^2/c^2)\widehat{G} = -\delta(x-x', y-y', z-z'), \tag{20}$$

which has Eq. (11) as its solution, subject to the property of boundedness as $R \to \infty$ in view of the condition of causality in the time domain. The right-hand side of Eq. (13) can be regarded as a *coordinate stretched 'spherical' wave*.

After multiplication of the left- and the right-hand sides by $\hat{\chi}_x\hat{\chi}_y\hat{\chi}_z$, the application of some standard rules of the unilateral Laplace transformation leads to the time-domain equivalent of Eq. (19):

$$\begin{aligned}\mathsf{D}^{\infty;\sigma}G^\sigma &\overset{\text{def}}{=} \chi_y(y,t) \overset{(t)}{*} \chi_z(z,t) \overset{(t)}{*} \partial_x(\chi_x^{-1}(x,t) \overset{(t)}{*} \partial_x G^\sigma) + \chi_z(z,t) \overset{(t)}{*} \chi_x(x,t) \overset{(t)}{*} \partial_y(\chi_y^{-1}(y,t) \overset{(t)}{*} \partial_y G^\sigma)\\ &\quad + \chi_x(x,t) \overset{(t)}{*} \chi_y(y,t) \overset{(t)}{*} \partial_z(\chi_z^{-1}(z,t) \overset{(t)}{*} \partial_z G^\sigma) - c^{-2}\partial_t^2(\chi_x(x,t) \overset{(t)}{*} \chi_y(y,t) \overset{(t)}{*} \chi_z(z,t) \overset{(t)}{*} G^\sigma)\\ &= -\delta(x-x', y-y', z-z', t),\end{aligned} \tag{21}$$

where $\chi_x^{-1}(x,t) \overset{(t)}{*} \chi_x(x,t) = \delta(t)$ for all x, with similar relations for $\chi_y^{-1}(y,t)$ and $\chi_z^{-1}(z,t)$. Since for $\boldsymbol{r} \neq \boldsymbol{r}'$ the derivatives of any order of $\widehat{G}^\sigma$ with respect to $\widehat{X}$, $\widehat{Y}$ and $\widehat{Z}$ exist, $\chi_x^{-1}(x,t) \overset{(t)}{*} \partial_x G^\sigma$ is piecewise continuously differentiable with respect to x, $\chi_y^{-1}(y,t) \overset{(t)}{*} \partial_y G^\sigma$ is piecewise continuously differentiable with respect to y and $\chi_z^{-1}(z,t) \overset{(t)}{*} \partial_z G^\sigma$ is piecewise continuously differentiable with respect to z. This has the consequence that any spatial stencil that can handle the discretization of D in Eq. (1), can also handle the discretization of the differential operator $\mathsf{D}^{\infty;\sigma}$, without having to be on the further alert for jumps in the quantities. Using the properties of G^σ as they follow from Eqs. (21) and (12) leads to

$$\mathsf{D}^{\infty;\sigma}u^\sigma = -Q^{\mathrm{i}} - Q^{\mathrm{s}} \quad \text{for } \boldsymbol{r} \in \mathbb{R}^3. \tag{22}$$

The domain in which the time-domain coordinate stretching functions differ from their values in the actual embedding will be denoted as the *Cartesian coordinate stretched perfectly matched embedding* (CartPME, for short) $\mathscr{E}^\sigma$:

$$\mathscr{E}^\sigma = \mathrm{supp}[\delta(t) - \chi_x(x,t)] \cup \mathrm{supp}[\delta(t) - \chi_y(y,t)] \cup \mathrm{supp}[\delta(t) - \chi_z(z,t)]. \tag{23}$$

For $\mathscr{E}^\sigma$ to act as an embedding of $\mathscr{D}$ (i.e., leaving the differential equation in $\mathscr{D}$ as it was), we must have $\mathscr{E}^\sigma \cap \mathscr{D} = \emptyset$.

Starting from the pertaining frequency-domain analysis, the role of time-convolution Cartesian coordinate stretching functions in the construction of PML's has also been discussed by Roden and Gedney [44]. Frequency-domain stretching functions associated with a complex Riemannian metric more general than the Cartesian one, have mathematically been discussed in [36,37].

4. The time-domain Cartesian coordinate-stretched dissipative wave equation

Based on the previous analysis, the time-domain, Cartesian coordinate-stretched dissipative wave operator D^σ becomes

$$\mathsf{D}^\sigma u^\sigma \stackrel{\mathrm{def}}{=} \partial_x(\mu_x^\sigma \overset{(t)}{*} \partial_x u^\sigma) + \partial_y(\mu_y^\sigma \overset{(t)}{*} \partial_y u^\sigma) + \partial_z(\mu_z^\sigma \overset{(t)}{*} \partial_z u^\sigma) - c^{-2}\kappa^\sigma \overset{(t)}{*} \partial_t^2 u^\sigma, \tag{24}$$

in which

$$\mu_x^\sigma = \begin{cases} \mu_x(\boldsymbol{r},t) & \text{for } \boldsymbol{r} \in \mathscr{D}, \\ \chi_x^{-1}(x,t) \overset{(t)}{*} \chi_y(y,t) \overset{(t)}{*} \chi_z(z,t) & \text{for } \boldsymbol{r} \in \mathscr{E}^\sigma, \end{cases} \tag{25}$$

$$\mu_y^\sigma = \begin{cases} \mu_y(\boldsymbol{r},t) & \text{for } \boldsymbol{r} \in \mathscr{D}, \\ \chi_y^{-1}(y,t) \overset{(t)}{*} \chi_z(z,t) \overset{(t)}{*} \chi_x(x,t) & \text{for } \boldsymbol{r} \in \mathscr{E}^\sigma, \end{cases} \tag{26}$$

$$\mu_z^\sigma = \begin{cases} \mu_z(\boldsymbol{r},t) & \text{for } \boldsymbol{r} \in \mathscr{D}, \\ \chi_z^{-1}(z,t) \overset{(t)}{*} \chi_x(x,t) \overset{(t)}{*} \chi_y(y,t) & \text{for } \boldsymbol{r} \in \mathscr{E}^\sigma, \end{cases} \tag{27}$$

$$\kappa^\sigma = \begin{cases} \kappa(\boldsymbol{r},t) & \text{for } \boldsymbol{r} \in \mathscr{D}, \\ \chi_x(x,t) \overset{(t)}{*} \chi_y(y,t) \overset{(t)}{*} \chi_z(z,t) & \text{for } \boldsymbol{r} \in \mathscr{E}^\sigma. \end{cases} \tag{28}$$

By combining Eqs. (4) and (22) with the definitions (25)–(28), it follows that

$$\mathsf{D}^\sigma u^\sigma = -Q^{\mathrm{i}} \quad \text{for } \boldsymbol{r} \in \mathscr{R}^3 \tag{29}$$

is the differential equation that reproduces the differential equation to be solved in the solution domain $\mathscr{D}$, while providing a perfectly matched outgoing wave propagation in the coordinate-stretched embedding $\mathscr{E}^\sigma$. Furthermore, we have $u^\sigma = u$ for $\boldsymbol{r} \in \mathscr{D}$ as it follows from Eqs. (5) and (12).

For practical use, a discretized version of Eq. (29) can only be employed in some subdomain $\mathscr{D} \cup \overline{\mathscr{E}^\sigma}$ of $\mathbb{R}^3$, where $\overline{\mathscr{E}^\sigma}$ is some truncated version of $\mathscr{E}^\sigma$. By the nature of the Cartesian coordinate stretching procedure, the total domain of computation is most advantageously taken to be a 3-rectangle with edges parallel to the axes of the chosen Cartesian reference frame, while having the solution domain $\mathscr{D}$ as a proper subset (Fig. 1). On the boundary surface $\partial\overline{\mathscr{E}^\sigma}$ of $\overline{\mathscr{E}^\sigma}$, explicit boundary conditions of either the Dirichlet or the Neumann type can then be invoked to generate the solution to the initial-/boundary-value problem associated with the equation

$$\mathsf{D}^\sigma u^\sigma = -Q^{\mathrm{i}} \quad \text{for } \boldsymbol{r} \in \mathscr{D} \cup \overline{\mathscr{E}^\sigma}. \tag{30}$$

The existence of solutions to this equation directly follows from our construction of the differential operator D^σ. The uniqueness of the relevant initial-/boundary-value problem remains, however, to be investigated.

5. Uniqueness of the coordinate-stretched initial-/boundary-value problem in a bounded domain

In relation to the uniqueness of the solution of the initial-/boundary-value problem associated with Eq. (30) in a bounded subdomain $\mathscr{D}^\sigma$ of $\mathbb{R}^3$, it is observed that in the theory of partial differential equations no direct time-domain uniqueness proofs are known to exist in case their terms contain time convolutions with the unknown functions and/or their derivatives, even if the (physical) restrictions of causality are laid upon them.

When expediting to the frequency domain, as is, for example, done in [46], the imposition on the constitutive coefficients of imaginary parts of the proper sign in addition to their positive real parts, yields indeed a sufficient condition for uniqueness for each frequency constituent separately, but even the imposition of the Kramers–Kronig relations between real and imaginary parts does not guarantee the (required) analyticity of the function involved in the right half $\mathrm{Re}(s) > 0$ of the complex s-plane [35]. An expedition into the time Laplace-transform domain, where causality has a one-to-one relationship with the analyticity properties of the transformed functions and Lerch's uniqueness theorem, seems at present the only tool to formulate necessary and sufficient conditions (see, [21] for elastodynamic and [20] for electromagnetic wave propagation and scattering problems in the presence of media with relaxation). For that reason such an approach is also followed here, upon subjecting the coordinate stretching functions, too, to the condition of causality.

We assume that $\mu_x^\sigma,\ \mu_y^\sigma,\ \mu_z^\sigma$ and κ^σ are piecewise continuous functions of $\boldsymbol{r}$, with possible finite jump discontinuities at a finite number of time-independent surfaces with a piecewise continuously turning normal, as well as piecewise continuous functions of time. An essential feature is furthermore that their Laplace transformed counterparts $\hat{\mu}_x^\sigma,\ \hat{\mu}_y^\sigma,\ \hat{\mu}_z^\sigma$ and $\hat{\kappa}^\sigma$ are analytic in the right half $\{s \in \mathbb{C}, \mathrm{Re}(s) > 0\}$ of the complex s-plane and real and positive for real, positive values of s, a subset of which is needed for the one-to-one correspondence between the time functions and their Laplace transforms. Across the surfaces of discontinuity in the coefficients, the coordinate-stretched wavefunction u^σ and its coordinate-stretched normal derivative $\boldsymbol{\nu} \cdot (\boldsymbol{\nabla}^\sigma \overset{(t)}{*} u^\sigma)$, where $\boldsymbol{\nabla}^\sigma = \mu_x^\sigma \boldsymbol{i}_x \partial_x + \mu_y^\sigma \boldsymbol{i}_y \partial_y + \mu_z^\sigma \boldsymbol{i}_z \partial_z$ and $\boldsymbol{\nu}$ is the unit vector along the normal to the surfaces, are to be continuous. Furthermore, the coordinate-stretched wavefunction is assumed to satisfy the initial conditions $u^\sigma(\boldsymbol{r}, 0) = 0$ and $\partial_t u^\sigma(\boldsymbol{r}, 0) = 0$ for all $\boldsymbol{r} \in \mathscr{D}^\sigma$. Under these conditions, $\partial_t^2 u^\sigma$ transforms into $s^2 \hat{u}^\sigma$. As to the boundary conditions on $\partial\mathscr{D}^\sigma$ we assume that $\partial\mathscr{D}^\sigma = \partial\mathscr{D}_{\mathrm{I}}^\sigma \cup \partial\mathscr{D}_{\mathrm{II}}^\sigma$, where on $\partial\mathscr{D}_{\mathrm{I}}^\sigma$ the value of u^σ is prescribed (Dirichlet condition), while on $\partial\mathscr{D}_{\mathrm{II}}^\sigma$ the value of $\boldsymbol{\nu} \cdot (\boldsymbol{\nabla}^\sigma \overset{(t)}{*} u^\sigma)$ (Neumann condition) is prescribed.

To prove uniqueness for the thus formulated initial-/boundary-value problem, we consider the Laplace-transformed counterpart of Eq. (29), i.e.,

$$\widehat{\mathrm{D}}^\sigma \hat{u}^\sigma = -\widehat{Q}^{\mathrm{i}} \quad \text{for } \boldsymbol{r} \in \mathscr{D}^\sigma, \tag{31}$$

in which

$$\widehat{\mathrm{D}}^\sigma \hat{u}^\sigma = \partial_x(\hat{\mu}_x^\sigma \partial_x \hat{u}^\sigma) + \partial_y(\hat{\mu}_y^\sigma \partial_y \hat{u}^\sigma) + \partial_z(\hat{\mu}_z^\sigma \partial_z(\hat{u}^\sigma) - (s/c)^{-2} \hat{\kappa}^\sigma \hat{u}^\sigma. \tag{32}$$

The spatial continuity conditions on the coefficients in the differential operator and those on the wavefuntion and its coordinate-stretched normal derivative carry over the time Laplace-transformed domain.

Let, now Δu^σ denote the difference between two possible solutions of the initial-/boundary-value problem under consideration, with the same prescribed source distributions in $\mathscr{D}^\sigma$ and the same boundary conditions on $\partial\mathscr{D}_{\mathrm{I}}^\sigma$ and $\partial\mathscr{D}_{\mathrm{II}}^\sigma$. Multiplying through in

$$\widehat{\mathrm{D}}^\sigma \Delta\hat{u}^\sigma = 0 \tag{33}$$

by $\Delta\hat{u}^\sigma$, integrating over $\mathscr{D}^\sigma$, manipulating with the derivatives, applying Gauss' divergence theorem and substituting the boundary conditions $\Delta\hat{u}^\sigma = 0$ (Dirichlet) on $\partial\mathscr{D}_{\mathrm{I}}^\sigma$ and $\boldsymbol{\nu} \cdot (\widehat{\boldsymbol{\nabla}}^\sigma \Delta\hat{u}^\sigma) = 0$ (Neumann) on $\partial\mathscr{D}_{\mathrm{II}}^\sigma$, we arrive at

$$\int_{\mathscr{D}^\sigma} [\hat{\mu}_x^\sigma (\partial_x \Delta\hat{u}^\sigma)^2 + \hat{\mu}_y^\sigma (\partial_y \Delta\hat{u}^\sigma)^2 + \hat{\mu}_z^\sigma (\partial_z \Delta\hat{u}^\sigma)^2 + (s/c)^2 \kappa^\sigma (\Delta\hat{u}^\sigma)^2] \,\mathrm{d}V = 0. \tag{34}$$

For any $\Delta\hat{u}^\sigma \not\equiv 0$ throughout $\mathscr{D}^\sigma$, all quantities being real-valued, the left-hand side of this equation is positive, which contradicts the value of its right-hand side. Consequently, $\Delta\hat{u}^\sigma \equiv 0$ throughout $\mathscr{D}^\sigma$, which proves uniqueness of $\hat{u}^\sigma$. On account of Lerch's uniqueness theorem of the Laplace transformation, then $\Delta u^\sigma \equiv 0$ throughout $\mathscr{D}^\sigma$, which completes the uniqueness proof for the time domain.

6. Scattering or contrast source formulation for a given incident wavefield

In those cases where the exciting sources of the wavefield are located in the embedding $\mathscr{D}^\infty$ at a large distance away from the contrasting regions in the solution domain $\mathscr{D}$, it is impractical to choose $\mathscr{D}$ to encompass

these sources, since it would unnecessarily increase the number of elements of discretization in $\mathscr{D}$. Since both the Green's function of the embedding $\mathscr{D}^\infty$ and the generating volume source densities are known, we can calculate the *incident wavefield* $u^{\mathrm{i}}(\boldsymbol{r},t)$ via (cf. Eq. (5))

$$u^{\mathrm{i}}(\boldsymbol{r},t)=\int_{\mathrm{supp}(Q^{\mathrm{i}})} G(\boldsymbol{r},\boldsymbol{r}',t)\overset{(t)}{*}Q^{\mathrm{i}}(\boldsymbol{r}',t)\,\mathrm{d}V(\boldsymbol{r}') \quad \text{for all } \boldsymbol{r}\in\mathbb{R}^3,\ t\in\mathbb{R}, \tag{35}$$

with G given by Eqs. (6) and (7). Next, we introduce the *scattered wavefield* $u^{\mathrm{s}}=u^{\mathrm{s}}(\boldsymbol{r},t)$ as

$$u^{\mathrm{s}}\overset{\mathrm{def}}{=}u-u^{\mathrm{i}} \quad \text{for all } \boldsymbol{r}\in\mathbb{R}^3,\ t\in\mathbb{R}. \tag{36}$$

Using the definitions of the operators D and D^∞ as given in Eqs. (1) and (2), the scattered wavefield is found to satisfy the differential equation

$$\mathsf{D}u^{\mathrm{s}}=(\mathsf{D}^\infty-\mathsf{D})u^{\mathrm{i}} \quad \text{for all } \boldsymbol{r}\in\mathbb{R}^3,\ t\in\mathbb{R}, \tag{37}$$

in which the support of the right-hand side is the contrasting subdomain of $\mathscr{D}$, i.e., the support of the *contrast sources*. Since u^{i} can be considered as known, the computational problem now amounts to solving Eq. (37) for u^{s} with the technique explained in Sections 3–5, after which the total wavefield follows as $u=u^{\mathrm{i}}+u^{\mathrm{s}}$. A limiting case arises when the exciting sources recede to infinity, in which case the incident wavefield reduces to a plane wave.

7. The sub-class of Cartesian coordinate-stretching functions invoking excess time delay and excess absorption

So far, the coordinate stretching functions that we have introduced are quite general as far as their dependence on space and time is concerned. In this section we more specifically demonstrate how the two major ingredients in the operation of perfectly matched embeddings, viz. *time delay* and *absorption* come into play. These two features show up in stretching profiles of the form

$$\chi_x(x,t)=[1+N_x(x)]\delta(t)+\sigma_x(x)H(t), \tag{38}$$

in which $N_x(x)\geqslant -1$, the *excess time-delay profile*, and $\sigma_x(x)\geqslant 0$, the *excess absorption profile*, are piecewise continuous functions of x, and $H(t)$ denotes the Heaviside unit step function. In view of the condition $\chi_x(x,t)\neq 0$ for $t\geqslant 0$, $1+N_x(x)$ and $\sigma_x(x)$ may not vanish simultaneously. Similar expressions apply to $\chi_y(y,t)$ and $\chi_z(z,t)$. The time-delay and absorption properties of these profiles as they manifest themselves in the solution to the coordinate-stretched wave equation, follow from substituting

$$\tilde{\chi}_x(x,s)=[1+N_x(x)]+s^{-1}\sigma_x(x), \tag{39}$$

and similar expressions for $\hat{\chi}_y(y,s)$ and $\hat{\chi}_z(z,s)$, in Eqs. (13)–(15). (For the equivalent frequency-domain construction, see [44].) This leads to

$$\widehat{G}^{\sigma}=\frac{s}{4\pi R_d}\frac{\exp\{-T_d[(s+\Gamma)^2+\Omega^2]^{1/2}\}}{[(s+\Gamma)^2+\Omega^2]^{1/2}} \quad \text{for } R_d\neq 0, \tag{40}$$

with

$$\begin{aligned} X_d&=\int_{x'}^{x}[1+N_x(\xi)]\,\mathrm{d}\xi, \quad Y_d=\int_{y'}^{y}[1+N_y(\eta)]\,\mathrm{d}\eta, \quad Z_d=\int_{z'}^{z}[1+N_z(\zeta)]\,\mathrm{d}\zeta,\\ X_a&=\int_{x'}^{x}\sigma_x(\xi)\,\mathrm{d}\xi, \quad Y_a=\int_{y'}^{y}\sigma_y(\eta)\,\mathrm{d}\eta, \quad Z_a=\int_{z'}^{z}\sigma_z(\zeta)\,\mathrm{d}\zeta, \end{aligned} \tag{41}$$

and

$$\begin{aligned} &R_d=(X_d^2+Y_d^2+Z_d^2)^{1/2}\geqslant 0, \quad R_a=(X_a^2+Y_a^2+Z_a^2)^{1/2}\geqslant 0, \quad T_d=R_d/c,\\ &\Gamma=(X_dX_a+Y_dY_a+Z_dZ_a)/R_d^2, \quad \Omega=(R_a^2/R_d^2-\Gamma^2)^{1/2}\geqslant 0. \end{aligned} \tag{42}$$

The corresponding time-domain result is [4]

$$G^\sigma = \partial_t\left[\frac{\exp(-\Gamma t)}{4\pi R_d} J_0[\Omega(t^2 - T_d^2)^{1/2}]H(t - T_d)\right] \quad \text{for } R_d > 0, \tag{43}$$

where J_0 is the Bessel function of the first kind and order zero. From this it is clear that T_d is the travel time of the coordinate-stretched wave function from the source point to the point of observation, Γ is the attenuation that the wave undergoes during its passage, while Ω is the angular frequency of oscillation induced by the coordinate stretching procedure (Γ and Ω both vanish for vanishing excess absorption).

In [35] it is argued that the second term in Eq. (39) presents a difficulty with respect to the Kramers–Kroning causality relations. The standard derivation of these relations assumes the imaginary s-axis to be free from singularities in the s-domain relaxation functions. If, however, the derivation is adapted to the presence of such singularities (in this case a simple pole at $s = 0$), the modified expressions are indeed representative (although not decisive) for causality. In fact, one can even go so far as to completely annihilate the wave propagation term in the CartPME by taking $N_x(x) = -1$, upon which a purely diffusive CartPME is left (see [5,46]). In this case, one has to take care to choose the time stepping in accordance with the resulting diffusive nature, rather than with wave propagation.

8. The point-source solution in the truncated coordinate-stretched configuration

The point-source solution in the truncated coordinate-stretched configuration provides an adequate tool to analyze the performance of the method. In the present section the structure of this solution is investigated for the case where the coordinate stretching procedure is carried out via the general relaxation procedure discussed in Section 3. Results for a specific case will be presented in Section 9.

The domain of computation is taken to be the 3-rectangle $\mathscr{D} \cup \overline{\mathscr{E}^\sigma}$ (Fig. 1). On the boundary $\partial\overline{\mathscr{E}^\sigma}$ of $\overline{\mathscr{E}^\sigma}$ we invoke the Dirichlet boundary condition $u^\sigma = 0$. In $\mathscr{D}$, a point source located at $\{x = x_0, y = y_0, z = z_0\}$ and source signature $f = f(t)$, with $f(t) = 0$ for $t < 0$, excites the configuration. The point-source solution in $\mathscr{D} \cup \overline{\mathscr{E}^\sigma}$ is constructed with the aid of the standard method of images. Let $\mathscr{D} \cup \overline{\mathscr{E}^\sigma}$ be given by $\{0 < x < a_x, 0 < y < a_y, 0 < z < a_z\}$, then we first continue this domain into the 3-rectangle $\{-a_x < x < a_x, -a_y < y < a_y, -a_z < z < a_z\}$ in which the constitutive coefficients are the mirror images of the ones in $\mathscr{D} \cup \overline{\mathscr{E}^\sigma}$, such that the planes $\{x = 0\}$, $\{y = 0\}$ and $\{z = 0\}$ are the planes of reflection symmetry. Next, we repeat the thus constructed pattern in $\{-a_x < x < a_x, -a_y < y < a_y, -a_z < z < a_z\}$ periodically with periods $2a_x$, $2a_y$ and $2a_z$ in the x-, y- and z-directions, respectively. The point-source solution in the thus continued configuration we denote as $G^\sigma(x, y, z; x_0, y_0, z_0; t)$. Then, the point-source solution in $\mathscr{D} \cup \overline{\mathscr{E}^\sigma}$ satisfying Dirichlet boundary conditions on $\partial\overline{\mathscr{E}^\sigma}$ is obtained as

$$u^\sigma = f(t) \overset{(t)}{*} \sum_{n_x,n_y,n_z} (-1)^{n_x+n_y+n_z} G_0^\sigma(x, y, z; x_0 + 2n_x a_x, y_0 + 2n_y a_y, z_0 + 2n_z a_z; t), \tag{44}$$

in which

$$\begin{aligned} G_0^\sigma(x, y, z; x_0, y_0, z_0; t) = {} & G^\sigma(x, y, z; x_0, y_0, z_0; t) - G^\sigma(x, y, z; x_0, y_0, -z_0; t) - G^\sigma(x, y, z; x_0, -y_0, z_0; t) \\ & + G^\sigma(x, y, z; x_0, -y_0, -z_0; t) - G^\sigma(x, y, z; -x_0, y_0, z_0; t) + G^\sigma(x, y, z; -x_0, y_0, -z_0; t) \\ & + G^\sigma(x, y, z; -x_0, -y_0, z_0; t) - G^\sigma(x, y, z; -x_0, -y_0, -z_0; t), \end{aligned} \tag{45}$$

all summations over the integers n_x, n_y and n_z running from $-\infty$ to ∞. For the solution domain $\mathscr{D}$ we take the 3-rectangle $\{d'_x < x < a_x - d''_x, d'_y < y < a_x - d''_y, d'_z < z < a_z - d''_z\}$, where $\{d'_x, \ldots, d''_z\} > \{0, \ldots, 0\}$ specify the thicknesses of the layers cut out of the 3D perfectly matched, Cartesian embedding in accordance with its computational truncation.

Each of the terms in Eq. (44), except the one corresponding to $n_x = 0$, $n_y = 0$, $n_z = 0$, gives rise to a spuriously reflected wavefield in the solution domain, with a time delay and/or an attenuation determined by the coordinate stretching relaxation functions it has encountered on its path of propagation in the embedding. Obviously, the most disturbing term is the image source closest to the source in the solution domain. Its decay across the pertinent part of the embedding can be used as a measure for the tolerance on the disturbing reflected waves in the solution domain. To illustrate what can be expected, we discuss in Section 9 a test case where all the relevant quantities can be evaluated analytically.

9. A test case with an analytical solution

For our test case we introduce in the perfectly matched embedding $\overline{\mathscr{E}^{\sigma}}$ 'left' and 'right' *excess time-delay* and *excess absorptive* profiles, where the 'left' excess time-delay profiles are of the type

$$N_{x;L}(x)=\left\{A^{N}_{x;L}\left(\frac{x_0-x}{x_0-x_L}\right)^{\nu^{N}_{x;L}}\exp\left(-\beta^{N}_{x;L}\frac{x-x_L}{x_0-x_L}\right),0\right\}\quad\text{for }\{x<x_0,x>x_0\}\tag{46}$$

and the 'left' *excess absorptive profile* of the type

$$\sigma_{x;L}(x)=\left\{A^{\sigma}_{x;L}\left(\frac{x_0-x}{x_0-x_L}\right)^{\nu^{\sigma}_{x;L}}\exp\left(-\beta^{\sigma}_{x;L}\frac{x-x_L}{x_0-x_L}\right),0\right\}\quad\text{for }\{x<x_0,x>x_0\},\tag{47}$$

in which $A^{N}_{x;L}$, $\nu^{N}_{x;L}$, $\beta^{N}_{x;L}$, $A^{\sigma}_{x;L}$, $\nu^{\sigma}_{x;L}$, $\beta^{\sigma}_{x;L}$ and are real-valued, non-negative parameters, x_0 is the x-coordinate where the coordinate stretching into the half-space $\{x<x_0\}$ starts and $x_L<x_0$ is the x-coordinate where the profile reaches the value $A^{N,\sigma}_{x;L}$. Similar expressions are taken for the profiles $N_{y;L}(y)$, $N_{z;L}(z)$, $\sigma_{y;L}(y)$ and $\sigma_{z;L}(z)$ and for the corresponding 'right' profiles. At the reference plane $\{x=x_L\}$, these profiles have the value $A_{N,\sigma}$, while they are continuous across the plane $\{x=x_0\}$ where the CartPME starts. (Note that this continuity seems to be preferred in computational implementations, although our analysis does not require it.) The value of $\nu_{N,\sigma}$ determines the behavior near $\{x=x_0\}$, the value of $\beta_{N,\sigma}$ determines the behavior as $x\to-\infty$. Fig. 2 illustrates this. Fig. 3(a)–(f) visualize how the propagation of the disturbance into the CartPME with excess time delay is slowed down and the propagation into an absorptive CartPME is attenuated, while illustrating that the corner yields no reflection at all. Fig. 3(d)–(f) illustrate the propagation into a CartPME with both time delay and absorption. All the different parameters in Eqs. (46) and (47) are at one's disposal to construct 3D perfectly matched Cartesian embeddings with a guaranteed time delay and/or attenuation, in accordance with a prescribed tolerance in the spuriously reflected wave. As such, the present special case can serve useful benchmark purposes in purely numerical implementations.

10. The computational system of differential equations

For the sub-class of coordinate stretching functions introduced in Section 7, a system of first-order space-time partial differential equations can be constructed that meets the requirement [24,48] that it can computationally be discretized in the same manner as applicable to standard wave equations in the solution domain, if necessary supplemented with a system of auxiliary ordinary differential equations in the time coordinate. Be it in a more ad-hoc manner, this was also the idea pursued in the pioneering split-field equations approach of Berenger [7–9]. The guiding principle for the construction of such a system can most easily inferred from

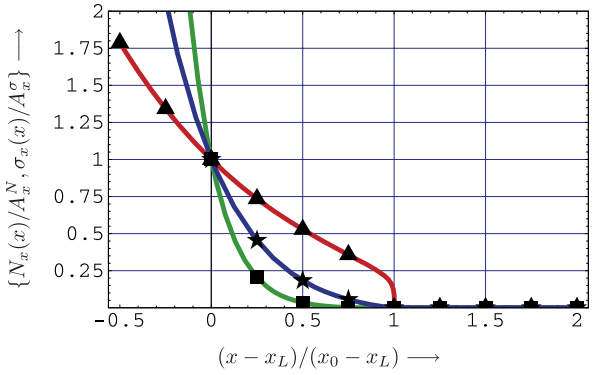

Fig. 2. Normalized Left excess time-delay and absorption profiles (▲: $A=1.0$, $\nu=0.5$, $\beta=1.0$; ■: $A=1.0$, $\nu=2.0$, $\beta=4.0$; ★: $A=1.0$, $\nu=1.0$, $\beta=2.0$).

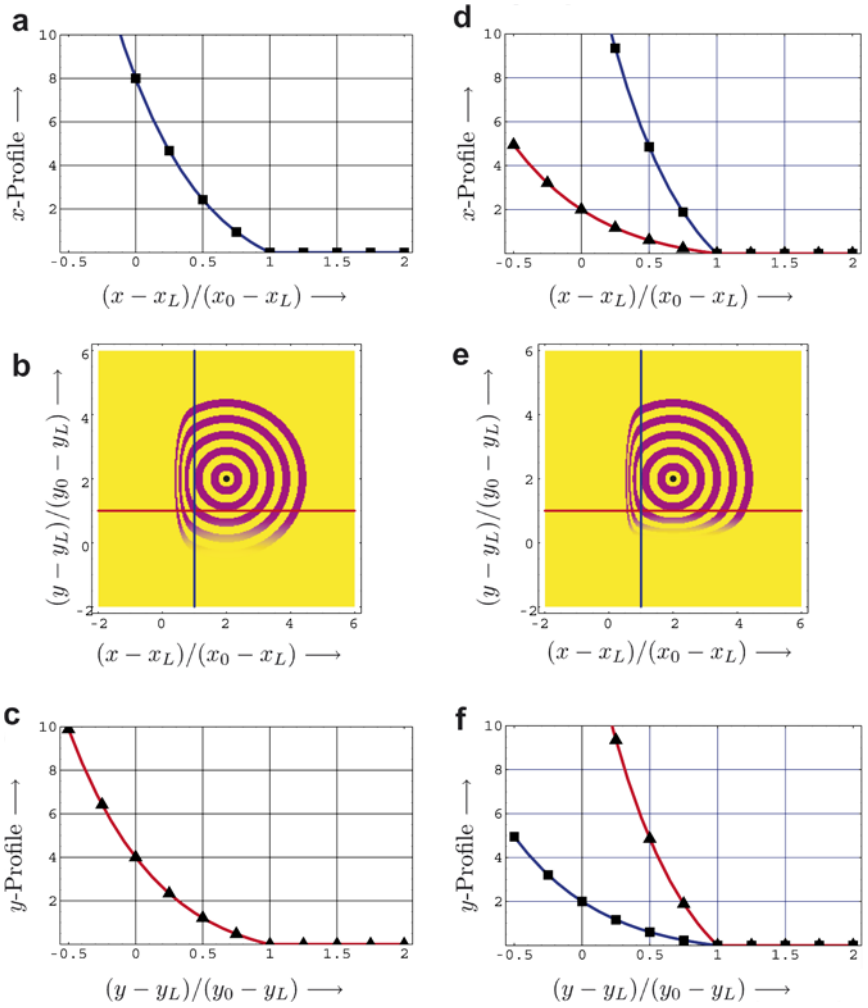

Fig. 3. (a) CartPME excess time-delay profile in x direction ($A_x^N = 8.0, v_x^N = 1.0, \beta_x^N = 1.0, A_x^\sigma = 0$); (b) Wavefronts at successive instants; (c) CartPME absorptive profile in y-direction ($A_y^\sigma = 4.0, v_y^\sigma = 1.0, \beta_y^\sigma = 1.0; A_y^N = 0$); (d) Predominantly time-delaying CartPME excess profile in x-direction (■ : $A_x^N = 16.0, v_x^N = 1.0, \beta_x^N = 1.0$; ▲ : $A_x^\sigma = 2.0, v_x^\sigma = 1.0, \beta_x^\sigma = 1.0$); (e) Wavefronts at successive instants; (f) Predominantly absorptive CartPME excess profile in y-direction (▲ : $A_y^\sigma = 16.0, v_y^\sigma = 1.0, \beta_y^\sigma = 1.0$; ■ : $A_y^N = 2.0, v_y^N = 1.0, \beta_y^N = 1.0$).

the time Laplace transform-domain coordinate-stretched wave equation in $\boldsymbol{r} \in \mathscr{D} \cup \overline{\mathscr{E}^\sigma}$ (the sources being present in $\mathscr{D}$). On account of Eq. (19) we have

$$\begin{aligned}&\hat{\chi}_x^{-1}\partial_x(\hat{\chi}_x^{-1}\partial_x\hat{u}^\sigma) + \hat{\chi}_y^{-1}\partial_y(\hat{\chi}_y^{-1}\partial_y\hat{u}^\sigma) + \hat{\chi}_z^{-1}\partial_z(\hat{\chi}_z^{-1}\partial_z\hat{u}^\sigma) - (s^2/c^2)\hat{u}^\sigma \\ &\quad = -(\hat{\chi}_x\hat{\chi}_y\hat{\chi}_z)^{-1}[\widehat{Q}^{\mathrm{i}}(\boldsymbol{r},s) + \widehat{Q}^{\mathrm{s}}(\boldsymbol{r},s)] \quad \text{for } \boldsymbol{r} \in \mathscr{D} \cup \overline{\mathscr{E}^\sigma}. \end{aligned} \tag{48}$$

Upon multiplying through by $\hat{\chi}_x(x,s)\hat{\chi}_y(y,s)\hat{\chi}_z(z,s)$ and introducing the computational unknown

$$\widehat{\widetilde{U}}(\boldsymbol{r},s) = \hat{\chi}_x(x,s)\hat{\chi}_y(y,s)\hat{\chi}_z(z,s)\hat{u}^\sigma(\boldsymbol{r},s), \tag{49}$$

we obtain

$$\begin{aligned}&\partial_x\left[\frac{1}{\hat{\chi}_x}\partial_x\left(\frac{1}{\hat{\chi}_x}\widehat{\widetilde{U}}\right)\right] + \partial_y\left[\frac{1}{\hat{\chi}_y}\partial_y\left(\frac{1}{\hat{\chi}_y}\widehat{\widetilde{U}}\right)\right] + \partial_z\left[\frac{1}{\hat{\chi}_z}\partial_z\left(\frac{1}{\hat{\chi}_z}\widehat{\widetilde{U}}\right)\right] - (s^2/c^2)\widehat{\widetilde{U}} \\ &\quad = -[\widehat{Q}^{\mathrm{i}}(\boldsymbol{r},s) + \widehat{Q}^{\mathrm{s}}(\boldsymbol{r},s)] \text{ for } \boldsymbol{r} \in \mathscr{D} \cup \overline{\mathscr{E}^\sigma}. \end{aligned} \tag{50}$$

A coupled first-order system of differential equations equivalent to (50) is

$$\partial_x \widehat{\widetilde{V}}_x + \partial_y \widehat{\widetilde{V}}_y + \partial_z \widehat{\widetilde{V}}_z - c^{-1}\partial_t \widetilde{U} = -\frac{c}{s}[\widehat{Q}^{\mathrm{i}}(\boldsymbol{r},s) + \widehat{Q}^{\mathrm{s}}(\boldsymbol{r},s)], \tag{51}$$

$$\partial_x \widehat{\widetilde{W}}_x - \frac{s}{c}\hat{\chi}_x \widehat{\widetilde{V}}_x = 0, \tag{52}$$

$$\partial_y \widehat{\widetilde{W}}_y - \frac{s}{c}\hat{\chi}_y \widehat{\widetilde{V}}_y = 0, \tag{53}$$

$$\partial_z \widehat{\widetilde{W}}_z - \frac{s}{c}\hat{\chi}_z \widehat{\widetilde{V}}_z = 0, \tag{54}$$

with the auxiliary equations

$$s\widehat{\widetilde{U}} - s\hat{\chi}_x \widehat{\widetilde{W}}_x = 0, \tag{55}$$

$$s\widehat{\widetilde{U}} - s\hat{\chi}_y \widehat{\widetilde{W}}_y = 0, \tag{56}$$

$$s\widehat{\widetilde{U}} - s\hat{\chi}_z \widehat{\widetilde{W}}_z = 0. \tag{57}$$

For profiles of the type (39) we have

$$s\hat{\chi}_x(x,s) = s[1 + N_x(x)] + \sigma_x(x), \tag{58}$$

with similar expressions for $\hat{\chi}_y(y,s)$ and $\hat{\chi}_z(z,s)$. Any factor of the type (58) transforms in the time domain into the operator

$$\partial_t \chi_x \overset{(t)}{*} = [1 + N_x(x)]\partial_t + \sigma_x(x), \tag{59}$$

with similar expressions for $\partial_t \chi_y(y,s) \overset{(t)}{*}$ and $\partial_t \chi_z(z,s) \overset{(t)}{*}$. From Eqs. (49)–(59) a coupled first-order system of space-time differential equations equivalent to (48) is then obtained as

$$\partial_x \widetilde{V}_x + \partial_y \widetilde{V}_y + \partial_z \widetilde{V}_z - c^{-1}\partial_t \widetilde{U} = -c\partial_t^{-1}[Q^{\mathrm{i}}(\boldsymbol{r},t) + Q^{\mathrm{s}}(\boldsymbol{r},t)], \tag{60}$$

$$\partial_x \widetilde{W}_x - c^{-1}\partial_t \chi_x \overset{(t)}{*} \widetilde{V}_x = 0, \tag{61}$$

$$\partial_y \widetilde{W}_y - c^{-1}\partial_t \chi_y \overset{(t)}{*} \widetilde{V}_y = 0, \tag{62}$$

$$\partial_z \widetilde{W}_z - c^{-1}\partial_t \chi_z \overset{(t)}{*} \widetilde{V}_z = 0, \tag{63}$$

with the auxiliary equations

$$\partial_t \widetilde{U} - \partial_t \chi_x \overset{(t)}{*} \widetilde{W}_x = 0, \tag{64}$$

$$\partial_t \widetilde{U} - \partial_t \chi_y \overset{(t)}{*} \widetilde{W}_y = 0, \tag{65}$$

$$\partial_t \widetilde{U} - \partial_t \chi_z \overset{(t)}{*} \widetilde{W}_z = 0, \tag{66}$$

in which

$$\partial_t \chi_x \overset{(t)}{*} = [1 + N_x(x)]\partial_t + \sigma_x(x), \tag{67}$$

$$\partial_t \chi_y \overset{(t)}{*} = [1 + N_y(y)]\partial_t + \sigma_y(y), \tag{68}$$

$$\partial_t \chi_x \overset{(t)}{*} = [1 + N_z(z)]\partial_t + \sigma_z(z) \tag{69}$$

and

$$\widetilde{U}(\boldsymbol{r},t) = \chi_x(x,t) \overset{(t)}{*} \chi_y(y,t) \overset{(t)}{*} \chi_z(z,t) \overset{(t)}{*} u(\boldsymbol{r},t) \tag{70}$$

that reduces to $u(\boldsymbol{r},t)$ in the original embedding $\mathscr{D}^{\infty}$. Eqs. (60)–(63) can be considered to be equivalents of the first-order coupled wave equations for acoustic waves in an anisotropic, lossy fluid [19, Section 4.5], while

Eqs. (64)–(66) are equivalent to the constitutive relations of such a fluid with frictional-force and compressibility relaxation loss behavior.

11. A 1D illustrative numerical example

Since for a number of simple CartPME profiles, an analytic solution to the problem is obtainable, it is worthwhile to carry out a numerical experiment to isolate the relative importance of spatial and temporal discretization errors, given a prescribed 'absorption capacity' of the CartPME. A thourough study in this respect is the recent publication by Sjögreen and Peterson [46]. (A corresponding study for the Helmholtz equation has been carried out in [45].) To restrict the number of parameters to play with, we consider a one-dimensional problem associated with the lossless scalar wave equation

$$\partial_x^2 u - c^{-2}\partial_t^2 u = -Q(t)\delta(x) \quad \text{for } -\infty < x < a_x, a_x > 0 \text{ (solution domain)}, \tag{71}$$

terminated with a 1D CartPME (i.e., a PML) of thickness d_x, provided with no excess time-delay profile, i.e.,

$$N_{x;L} = 0, \tag{72}$$

and a cubic absorption profile

$$\sigma_{x;L}(x) = \left\{0, A^{\sigma}_{x;L}\left(\frac{x-a_x}{d_x}\right)^3\right\} \quad \text{for } \{-\infty < x < a_x, a_x \leqslant x \leqslant a_x + d_x\}, A^{\sigma}_{x;L} > 0, d_x > 0. \tag{73}$$

A Dirichlet boundary condition is invoked at $x = a_x + d_x$:

$$u(x,t) = 0 \quad \text{for } x = a_x + d_x. \tag{74}$$

The solution to the s-domain counterpart of this problem is

$$\hat{u}(x,s) = \widehat{Q}(s)\frac{c}{2s}\exp\left[\frac{s}{c}x\right] - \widehat{Q}(s)\frac{c}{2s}\exp\left[-\frac{s}{c}\int_{\xi=x}^{2(a_x+d_x)}[1+N(\xi)]\mathrm{d}\xi - \frac{1}{c}\int_{\xi=x}^{2(a_x+d_x)}\sigma(\xi)\mathrm{d}\xi\right] \quad \text{for } -\infty < x < 0, \tag{75}$$

$$\begin{aligned}\hat{u}(x,s) = {} & \widehat{Q}(s)\frac{c}{2s}\exp\left[-\frac{s}{c}\int_{\xi=0}^{x}[1+N(\xi)]\mathrm{d}\xi - \frac{1}{c}\int_{\xi=0}^{x}\sigma(\xi)\mathrm{d}\xi\right] \\ & - \widehat{Q}(s)\frac{c}{2s}\exp\left[-\frac{s}{c}\int_{\xi=x}^{2(a_x+d_x)}[1+N(\xi)]\mathrm{d}\xi - \frac{1}{c}\int_{\xi=x}^{2(a_x+d_x)}\sigma(\xi)\mathrm{d}\xi\right] \quad \text{for } 0 < x < a_x + d_x.\end{aligned} \tag{76}$$

This leads to the time-domain expressions

$$u(x,t) = \frac{c}{2}\partial_t^{-1}Q\left(t+\frac{x}{c}\right) - \frac{c}{2}\exp\left[-\frac{1}{c}\int_{\xi=x}^{2(a_x+d_x)}\sigma(\xi)\mathrm{d}\xi\right]\partial_t^{-1}Q\left[t-\frac{1}{c}\int_{\xi=x}^{2(a_x+d_x)}[1+N(\xi)]\mathrm{d}\xi\right] \quad \text{for } -\infty < x < 0, \tag{77}$$

$$\begin{aligned}u(x,t) = {} & \frac{c}{2}\exp\left[-\frac{1}{c}\int_{\xi=0}^{x}\sigma(\xi)\mathrm{d}\xi\right]\partial_t^{-1}Q\left[t-\frac{1}{c}\int_{\xi=0}^{x}[1+N(\xi)]\mathrm{d}\xi\right] \\ & - \frac{c}{2}\exp\left[-\frac{1}{c}\int_{\xi=x}^{2(a_x+d_x)}\sigma(\xi)\mathrm{d}\xi\right]\partial_t^{-1}Q\left[t-\frac{1}{c}\int_{\xi=x}^{2(a_x+d_x)}[1+N(\xi)]\mathrm{d}\xi\right] \quad \text{for } 0 < x < a_x + d_x,\end{aligned} \tag{78}$$

where ∂_t^{-1} denotes time integration. Results are presented for the source signature (Fig. 4a)

$$Q(t) = Q_0\frac{2}{ct_{\mathrm{r}}}(1 - t/t_{\mathrm{r}})\exp(-t/t_{\mathrm{r}} + 1)H(t), \tag{79}$$

that leads to the excitation of the unipolar pulse (Fig. 4b)

$$u(t) = u_0(t/t_{\mathrm{r}})\exp(-t/t_{\mathrm{r}} + 1)H(t), \tag{80}$$

of *pulse rise time* t_{r} and *pulse time width* $t_{\mathrm{w}} = t_{\mathrm{r}}\exp(1)$.

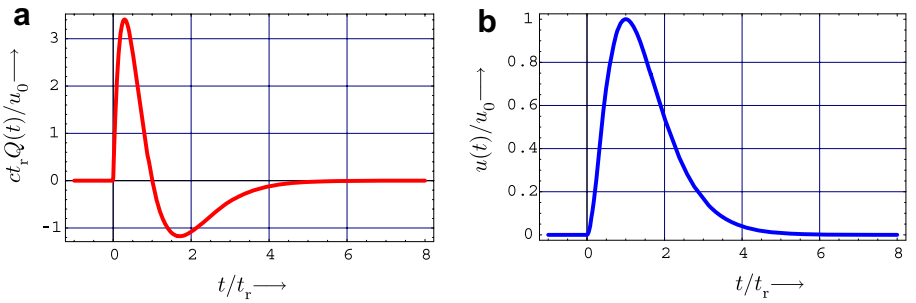

Fig. 4. 1D CartPME configuration: (a) source signature and (b) generated wave shape.

To extract the discretization error, the 1D equivalent of the system of Eqs. (60)–(70) (with $\partial_y = 0, \partial_z = 0$, $W_y = 0, W_z = 0, V_y = 0, V_z = 0$) has been solved via a standard staggered-grid space-time discretization scheme, the mesh sizes of which are shown in Table 1. For all curves, the time step is taken to be $\Delta t = t_r/200$. The absorption properties of the layer are expressed via the cubic power law amplitude reflection coefficient $\rho = \exp(-A^{\sigma}_{x;L} d_x/4)$ of the spuriously reflected wave. Fig. 5 shows a few results in their dependence on the parameters of an absorptive CartPME without excess time delay. The indicated values of ρ are chosen such that, on the scale of the figure, there remains something to be seen. In each case, the sampling of the layer takes place at ten equidistant intervals.

Table 1
Numerical reflection factor ρ_{num} for $\Delta t = 0.95\Delta x$ and $d = N_{\text{PML}}\Delta x$

$\rho = 10^{-1}$			$\rho = 10^{-2}$			$\rho = 10^{-3}$		
N_{PML}	ρ_{num}	Rel. error	N_{PML}	ρ_{num}	Rel. error	N_{PML}	ρ_{num}	Rel. error
1	2.695×10^{-1}	1.695	1	7.058×10^{-2}	6.058	1	2.668×10^{-1}	2.658×10^{2}
5	1.068×10^{-1}	6.829×10^{-2}	5	1.303×10^{-2}	3.034×10^{-1}	5	2.192×10^{-3}	1.192
10	1.020×10^{-1}	2.035×10^{-2}	10	1.099×10^{-2}	9.928×10^{-2}	10	1.427×10^{-3}	4.273×10^{-1}
15	1.010×10^{-1}	9.886×10^{-3}	15	1.053×10^{-2}	5.339×10^{-2}	15	1.284×10^{-3}	2.841×10^{-1}
20	1.006×10^{-1}	5.984×10^{-3}	20	1.035×10^{-2}	3.486×10^{-2}	20	1.230×10^{-3}	2.300×10^{-1}

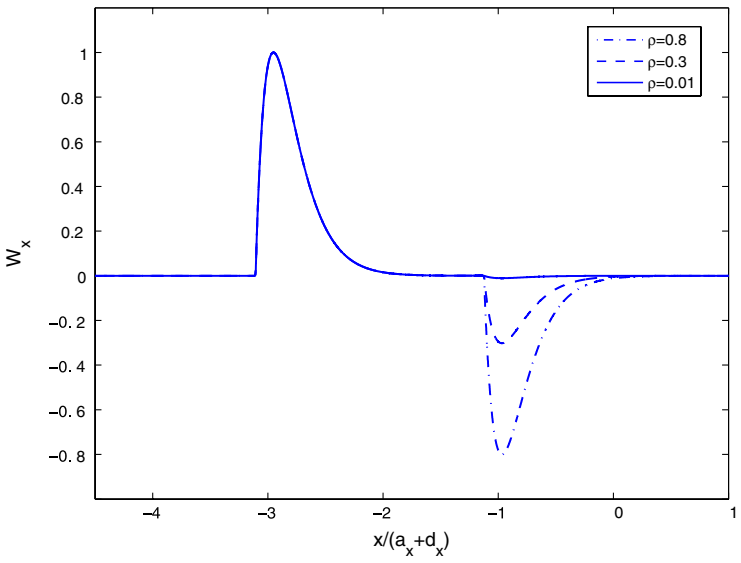

Fig. 5. Numerical results for a 1D wave reflected against a Dirichlet boundary condition truncated 1D CartPME.

In Table 1, more refined values are given for the absolute numerical error in the wave functions as they are computed with an FDTD-code, with time and space steps as indicated. It is observed that no difficulties arise at late times, notwithstanding the fact that absorption is the main action of the CartPME under consideration.

12. Conclusion

A methodology is presented for constructing a class of 3D perfectly matched embeddings for the space-time partial differential equations associated with time-domain wave motion computation. Based upon the contrast-source formulation of the wave field problem with respect to a homogeneous embedding, the key issue in the procedure is the construction of the relevant time-domain Green's function in the configuration consisting of computational *solution domain*, surrounded by a Cartesian coordinate stretched perfectly matched embedding. The coordinate stretching procedure goes via time-convolutional stretching functions that preserve causality and passivity, and therefore uniqueness of the time-domain problem. A particular subclass of stretching functions is shown to lead to a combined time delay and absorption in the embedding, with parameters that are adjustable to satisfy user-defined accuracy requirements on the solution in the solution domain, insofar these are related to the spuriously reflected wave that is generated by the (computationally unavoidable) truncation of the embedding and the imposition of Dirichlet or Neumann boundary conditions on the pertaining walls. Also for this subclass, the pertaining system of equivalent differential equations is given that avoids the computation of the time convolutions in the original coordinate-stretched differential equation. Numerical results are shown for a class of profiles where the spuriously reflected wave generated by a point source can be calculated analytically. The Green's function approach in general reveals properties of the solution to the problem, irrespective of a particular space-time discretization procedure used to solve the relevant differential equations.

Acknowledgement

The authors would like to thank the (anonymous) reviewers for their careful reading of the manuscript, their constructive criticism and their suggestions for improvement of the paper.

Appendix A. Quasi-static behavior

The late-time behavior of transient wave motion [2] is often brought in relation to the quasi-static behavior of the pertaining wave equation. From the time-domain equation this behavior is to follow upon deleting the terms that contain the partial derivatives with respect to t, while in the corresponding complex frequency domain equations one puts the complex frequency (time Laplace transform parameter) s equal to zero. The interrelation of these operations with late time behavior rests on the applicability of the relevant Abel theorems of the unilateral time Laplace transformation [51]. The validity of the relevant procedure is, here too, closely related to the behavior of the Green's function. As easily follows from the procedure discussed in Section 3, the s-domain coordinate-stretched Green's function of the 1D wave equation with wave speed c is $\widehat{G}^{\sigma;\mathrm{I}}(x,x',s) = (c/2s)\exp[-(s/c)R^{\sigma;\mathrm{I}}]$, the one for the 2D wave equation is $\widehat{G}^{\sigma;\mathrm{II}}(\boldsymbol{r},\boldsymbol{r}',s) = (2\pi)^{-1}K_0[(s/c)R^{\sigma;\mathrm{II}}]$, where K_0 is the modified Bessel function of the second kind and order zero, while, as shown, the one for the 3D wave equation is $\widehat{G}^{\sigma;\mathrm{III}}(\boldsymbol{r},\boldsymbol{r}',s) = (4\pi R^{\sigma;\mathrm{III}})^{-1}\exp[-(s/c)R^{\sigma;\mathrm{III}}]$, where $R^{\sigma;\mathrm{I,II,III}}$ is the coordinate-stretched 1D, 2D and 3D distance function, respectively. Only $\widehat{G}^{\mathrm{III}}$ is regular at $s=0$ and the reasoning sketched above does apply. However, $\widehat{G}^{\mathrm{I}}$ has a simple pole at $s=0$ and $\widehat{G}^{\mathrm{II}}$ has a logarithmic branch point at $s=0$, which singularities withstand a straightforward application of the Abel theorems. This, again, shows that at least some properties of the solutions of coordinate-stretched wave equations are not directly evident from the differential equations, but clearly show up in the corresponding Green's functions.

References

[1] S. Abarbanel, D. Gottlieb, A mathematical analysis of the PML method, Journal of Computational Physics 134 (1997) 357–363.
[2] S. Abarbanel, D. Gottlieb, J.S. Hesthaven, Long time behavior of the perfectly matched layer equations in computational electromagnetics, Journal of Scientific Computing 17 (2002) 405–422.

[3] S. Abarbanel, D. Gottlieb, On the construction and analysis of absorbing layers in CEM, Applied Numerical Mathematics 27 (1998) 331–340.
[4] M. Abramowitz, I.A. Stegun, Handbook of Mathematical Functions, Dover Publications, New York, 1965, p. 1027.
[5] S. Asvadurov, V. Druskin, M.N. Gudatti, L. Knizhnerman, On optimal finite-difference approximation of PML, SIAM Journal of Numerical Analysis 41 (2003) 28–305.
[6] E. Bécache, S. Fauqueux, P. Joly, Stability of perfectly matched layers, group velocities and anisotropic waves, Journal of Computational Physics 188 (2003) 399–433.
[7] J.P. Berenger, A perfectly matched layer for the absorption of electromagnetic waves, Journal of Computational Physics 114 (1994) 185–200.
[8] J.P. Berenger, Evanescent waves in PML's: Origin of the numerical reflection in wave–structure interaction problems, IEEE Transactions on Antennas and Propagation 47 (1999) 1497–1503.
[9] J.P. Berenger, Numerical reflection from FDTD-PMLs: A comparison of the split PML with the unsplit and CFS PMLs, IEEE Transactions on Antennas and Propagation 50 (2002) 258–265.
[10] C. Cerjan, D. Kosloff, R. Kosloff, M. Reshev, A nonreflecting boundary condition for discrete acoustic and elastic wave equations, Geophysics 50 (1985) 705–708.
[11] Y.H. Chen, W.C. Chew, M.L. Oristaglio, Application of perfectly matched layers to the transient modeling of subsurface EM problems, Geophysics 62 (1997) 1730–1736.
[12] W.C. Chew, J.M. Jin, Perfectly matched layers in the discretized space: Analysis and optimization, Electromagnetics 16 (1996) 325–340.
[13] W.C. Chew, W.M. Jin, E. Michielssen, Complex coordinate stretching as a generalized absorbing boundary condition, Microwave and Optical Technology Letters 15 (1997) 363–369.
[14] W.C. Chew, J.M. Jin, E. Michielssen, J. Song, Fast and Efficient Algorithms in Computational Electromagnetics, Artech House, Boston, 2001, Chapter 7.
[15] W.C. Chew, Q.H. Liu, Perfectly matched layers for elastodynamics: A new absorbing boundary condition, Journal of Computational Acoustics 4 (1996) 72–79.
[16] W.C. Chew, W.H. Weedon, A 3D perfectly matched medium from modified Maxwell equations with stretched coordinates, Microwave Optics and Technology Letters 7 (1994) 599–604.
[17] R.M. Christensen, Theory of Viscoelasticity, 2nd ed. Dover Publications, Mineola, N.Y.
[18] F. Collino, P. Monk, The perfectly matched layer in curvilinear coordinates, SIAM Journal of Scientific Computing 19 (1998) 2061–2090.
[19] A.T. de Hoop, Handbook of Radiation and Scattering of Waves, Academic Press, London, 1995.
[20] A.T. de Hoop, A time-domain uniqueness theorem for electromagnetic wavefield modelling in dispersive, anisotropic media, The Radio Science Bulletin 305 (2003) 17–21.
[21] A.T. de Hoop, A uniqueness theorem for the time-domain elastic-wave scattering in inhomogeneous, anisotropic solids with relaxation, The Journal of the Acoustical Society of America 115 (2004) 2711–2715.
[22] A.T. de Hoop, P.M. van den Berg, R.F. Remis, Analytic time-domain performance analysis of absorbing boundary conditions and perfectly matched layers, in: 2001 IEEE AP-S International Symposium and USNC/URSI National Radio Science Meeting, Boston, USA, 08–13 July 2001, vol. IV, pp. 502–505.
[23] A.T. de Hoop, P.M. van den Berg, R.F. Remis, Absorbing boundary conditions and perfectly matched layers – An analytic time-domain performance analysis, IEEE Transactions on Magnetics 38 (2002) 657–660.
[24] S.D. Gedney, A. Tavlove, Perfectly Matched Layer Absorbing Boundary Conditions, in: A. Tavlove, S.C. Hagness (Eds.), Computational Electrodynamics: The Finite-Difference Time-Domain Method, second ed., Artech House, Boston, 2000, Chapter 7.
[25] S.D. Gedney, G. Liu, J.A. Roden, A. Zhu, Perfectly matched layer media with CFS for an unconditionally stable ADI-FDTD method, IEEE Transactions on Antennas and Propagation 49 (2001) 1554–1559.
[26] D. Givoli, J.B. Keller, Nonreflecting boundary conditions for elastic waves, Wave Motion 12 (1990) 261–279.
[27] M.J. Grote, J.B. Keller, Exact nonreflecting boundary conditions for the time dependent wave equation, SIAM Journal of Applied Mathematics 55 (1995) 280–297.
[28] M.J. Grote, J.B. Keller, Nonreflecting boundary conditions for time dependent scattering, Journal of Computational Physics 127 (1996) 52–65.
[29] M.J. Grote, J.B. Keller, Nonreflecting boundary conditions for Maxwell's equations, Journal of Computational Physics 139 (1998) 327–342.
[30] M.J. Grote, J.B. Keller, Exact nonreflecting boundary condition for elastic waves, SIAM Journal of Applied Mathematics 60 (2000) 803–819.
[31] F.D. Hastings, J.B. Schneider, S.L. Broschat, Application of the Perfectly Matched Layer (PML) absorbing boundary condition for elastic wave propagation, The Journal of the Acoustical Society of America 100 (1996) 3061–3069.
[32] D. Jiao, J-M. Jin, An effective algorithm for implementing perfectly matched layers in time-domain finite-element simulation of open-region EM problems, IEEE Transactions on Antennas and Propagation 50 (2002) 1615–1623.
[33] D. Jiao, J-M. Jin, E. Michielssen, Time-domain finite-element simulation of three-dimensional scattering and radiation problems using perfectly matched layers, IEEE Transactions on Antennas and Propagation 51 (2003) 296–305.
[34] J.B. Keller, D. Givoli, Exact nonreflecting boundary conditions, Journal of Computational Physics 82 (1989) 172–192.
[35] M. Kozuoglu, R. Mittra, A systematic study of perfectly matched absorbers, in: D.H. Werner, R. Mittra (Eds.), Frontiers in Electromagnetics, IEEE Press, New York, 2000, Chapter 14.

[36] M. Lassas, E. Somersalo, Analysis of the PML equations in general convex geometry, Proceedings of the Royal Society of Edinburgh 131A (2001) 1183–1207.
[37] M. Lassas, J. Liukkonen, E. Somersalo, Complex Riemannian metric and absorbing boundary conditions, Journal de Mathématiques Pures et Appliquées 80 (2001) 739–768.
[38] Q.H. Liu, Perfectly matched layers for elastic waves in cylindrical and spherical coordinates, The Journal of the Acoustical Society of America 105 (1999) 2075–2084.
[39] Q.H. Liu, J.Q. He, Quasi-PML for waves in cylindrical coordinates, Microwave and Optics Technology Letters 19 (1996) 107–111.
[40] Q.H. Liu, J. Tao, The Perfectly Matched Lyaer (PML) for acoustic waves in absorptive media, The Journal of the Acoustical Society of America 102 (1997) 2072–2082.
[41] P.G. Petropoulos, Reflectionless sponge layers as absorbing boundary conditions for the numerical solution of Maxwell equations in rectangular, cylindrical, and spherical coordinates, SIAM Journal of Applied Mathematics 60 (2000) 1037–1058.
[42] C.M. Rappaport, Perfectly matched absorbing boundary conditions based on anisotropic lossy mapping of space, IEEE Microwave and Guided Wave Letters 5 (1995) 90–92.
[43] C.M. Rappaport, L. Bahrmasel, An absorbing boundary condition based on anechoic absorber for EM scattering computation, Journal of Electromagneitc Waves and Applications 6 (1992) 1621–1634.
[44] J.A. Roden, S.D. Gedney, Convolution PML (CPML): an efficient FDTD implementation of the CFD-PML for arbitrary media, Microwave and Optical Technology Letters 27 (2000) 334–339.
[45] I. Singer, E. Turkel, A perfectly matched layer for the Helmholtz equation in a semi-infinite strip, Journal of Computational Physics 201 (2004) 439–465.
[46] B. Sjögreen, N.A. Petersson, Perfectly matched layers for Maxwell's equations in second order formulation, Journal of Computational Physics 209 (2005) 19–46.
[47] A. Tavlove, Advances in Computational Electrodynamics: The Finite-Difference Time-Domain Method, Artech House, Boston, 1998, Chapter 5.
[48] A. Tavlove, S.C. Hagness, Computational Electrodynamics: The Finite-Difference Time-Domain Method, second ed., Artech House, Boston, 2000, Chapter 9.
[49] F.L. Teixeira, K.-P. Hwang, W.C. Chew, J.-M. Jin, Conformal PML-FDTD schemes for electromagnetic field simulations: a dynamic stability study, IEEE Transactions on Antennas and Propagation 49 (2001) 902–907.
[50] E. Turkel, A. Yefet, Absorbing PML boundary layers for wave-like equations, Applied Numerical Mathematics 27 (1998) 533–557.
[51] B. van der Pol, H. Bremmer, Operational Calculus based on the two-sided Laplace Integral, Cambridge University Press, Cambridge, UK, 1950, Section VII.3.
[52] D.V. Widder, The Laplace Transform Princeton, University Press, Princeton, NJ, 1946, p. 63.
[53] X. Yuan, D. Borup, J.W. Wiskin, M. Berggren, R. Eidens, S.A. Johnson, Formulation and validation of Berenger's PML absorbing boundary for the FDTD simulation of acoustic scattering, IEEE Transactions on Ultrasonics, Ferroelectrics and Frequency Control 44 (1997) 816–822.